

# Optical emission line profiles of the LV knots (proplyds) in Orion

W.J. Henney<sup>1</sup>, J. Meaburn<sup>2</sup>, A.C. Raga<sup>1</sup>, and R. Massey<sup>2</sup>

<sup>1</sup> Instituto de Astronomía, UNAM, Apartado Postal 70–264, 04510 México D.F., México

<sup>2</sup> Department of Physics and Astronomy, The University, Manchester M13 9PL, UK

Received 31 July 1996 / Accepted 11 December 1996

**Abstract.** Compact emission line “LV knots” discovered by Laques and Vidal (1979) in the Orion Nebula (M 42) are found to spatially coincide with some of the “proplyds” discovered by O’Dell, Wen and Hu (1993) in their HST images. We therefore attempt to reproduce the line profiles observed for the LV knots with the photoevaporated disk/wind interaction model that has been developed by Henney et al. (1996) for modelling the proplyds.

In particular, we present high resolution [O III] 5007Å line profiles of the knots LV 1 (OW 168–326E), LV 2 (OW 167–317), LV 3 (OW 163–317) and LV 5 (OW 158–323), and also of another faint emission line knot (OW 171–334) in the vicinity of  $\theta^1$  Ori C. Good agreement between the theoretical predictions and the observed line profiles is found for three of the knots, in which most of the main features of the line profiles are reproduced by the model. A partial, qualitative agreement is also found for the other knots.

From these results we conclude that the model of a photoevaporated disk wind interacting with the wind from  $\theta^1$  Ori C at least partially succeeds in reproducing the line profiles of the proplyds associated with the LV knots.

**Key words:** ISM: H II regions – ISM: Individual: Orion nebula – ISM: jets and outflows – line: profiles – stars: pre-main-sequence

## 1. Introduction

Compact emission line knots were discovered by Laques and Vidal (1979) in the central region of the Orion nebula (M 42, NGC 1976), within 10'' from  $\theta^1$  Ori C. These knots (LV 1–6) and many others have been detected in the thermal radio continuum by Garay, Moran and Reed (1987), Churchwell et al. (1987) and by Felli et al. (1993). Optical and infrared continuum emission indicating the presence of central stars within these knots has been detected (Meaburn 1988; McCaughrean 1988; McCaughrean & Stauffer 1994).

The HST images of the LV knots by O’Dell, Wen and Hu (1993) and O’Dell and Wen (1994) show a number to have a

cometary shape. The “tails” of these knots point away from  $\theta^1$  Ori C, and have a spatial distribution approximately centred on this star. These knots were named “proplyds” (for “proto-planetary disks”) by O’Dell, Wen and Hu (1993), who suggested that they were associated with disks around low mass stars that were interacting with the ionizing radiation field and possibly also with the wind from  $\theta^1$  Ori C.

Henney et al. (1996) (Paper I) have recently developed an analytic model for a disk around a low mass star that is being photoevaporated by the radiation field of an external O star. The photoevaporated wind is then driven back by the wind from the O star, forming a “head/tail”, cometary structure. This model is successful in reproducing qualitatively the HST images of the proplyds, as well as the size and H $\alpha$  luminosity vs. distance (from  $\theta^1$  Ori C) correlations found by McCullough et al. (1995) for these objects.

However, it would clearly be interesting to see if these models could also explain the kinematical properties of the proplyds. It is possible to do this quite straightforwardly because some of the proplyds correspond to the LV knots, for which detailed, high-dispersion spectroscopic studies have been carried out in the past (Meaburn 1988; Meaburn et al. 1993; Massey and Meaburn 1993, 1995).

In this paper, we present a comparison between the high dispersion [O III] 5007Å line profiles of the LV knots (extracted from the observations of Massey & Meaburn 1995) and predictions from the models of Paper I. In the following section we discuss the similarities and differences between the predicted line profiles, and the observations of the knots LV 1 (OW 168–326E), LV 2 (OW 167–317), LV 3 (OW 163–317) and LV 5 (OW 158–323), and also of another emission-line knot (OW 171–334) in the same region (also found to be a proplyd).

## 2. Predicted and observed [O III] line profiles

### 2.1. Observations

Longslit spectrographic observations were carried out with the Manchester Echelle Spectrometer on the 2.5 m Isaac Newton Telescope between 1991 and 1993. Full details of the observational setup are reported in Massey & Meaburn (1995). In this paper, we present the extracted spectra of five emission line

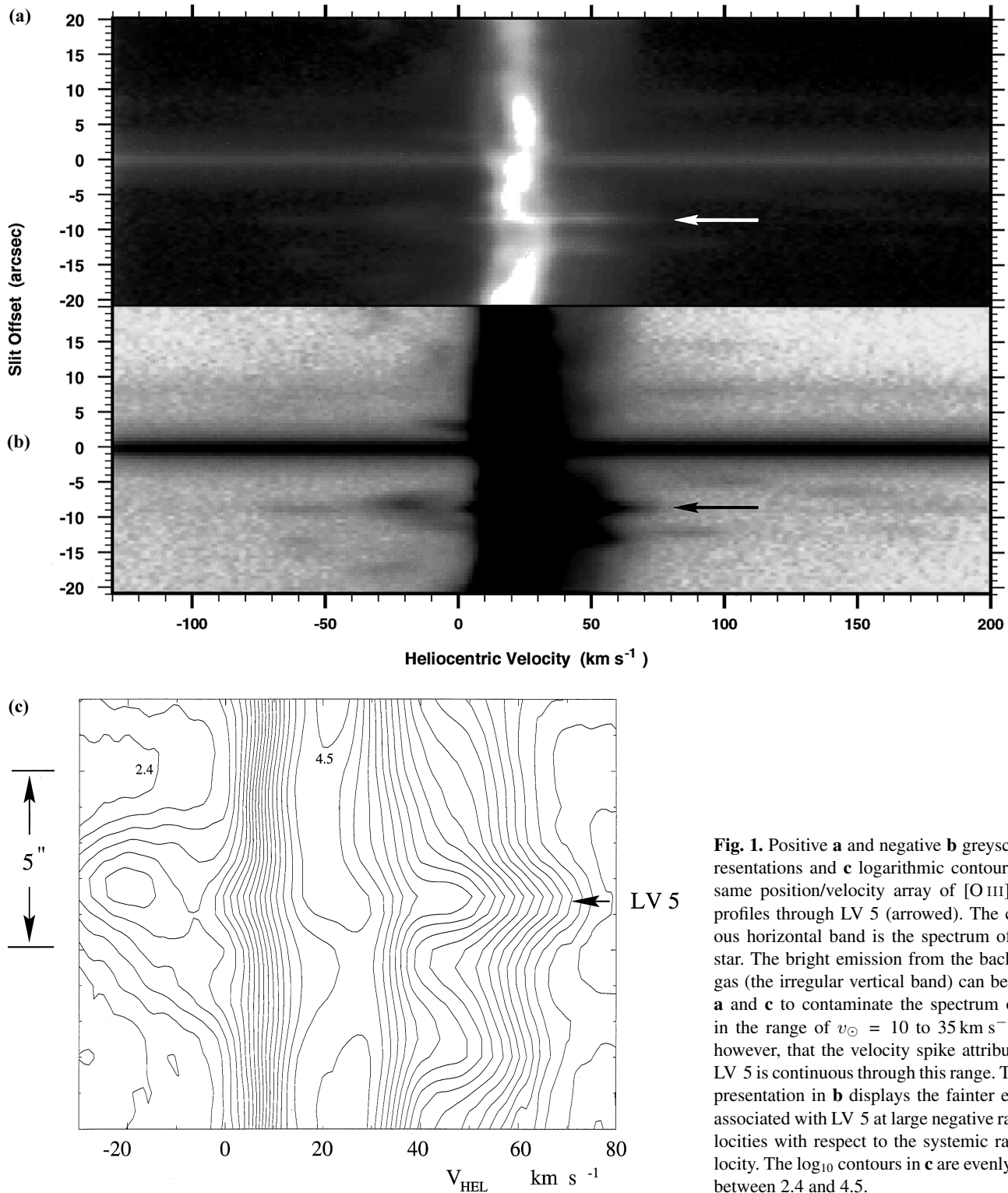


**Fig. 1.** Positive **a** and negative **b** greyscale representations and **c** logarithmic contours of the same position/velocity array of [O III] 5007Å profiles through LV 5 (arrowed). The continuous horizontal band is the spectrum of a field star. The bright emission from the background gas (the irregular vertical band) can be seen in **a** and **c** to contaminate the spectrum of LV 5 in the range of  $v_{\odot} = 10$  to  $35 \text{ km s}^{-1}$ . Note, however, that the velocity spike attributable to LV 5 is continuous through this range. The deep presentation in **b** displays the fainter emission associated with LV 5 at large negative radial velocities with respect to the systemic radial velocity. The  $\log_{10}$  contours in **c** are evenly spaced between 2.4 and 4.5.

knots (proplyds), which are listed in Table 1, together with the observational parameters for each object.

In each case, an attempt was made to isolate the emission due to the proplyd itself from that due to the nebular background. This was more successful in some cases than in others. For LV 5 (OW 158–323), excellent seeing resulted in relatively

straightforward background subtraction and we are confident that in this case all the features in the spectrum outside of the narrow range  $v_{\odot} = 10$ – $35 \text{ km s}^{-1}$  belong to the emission knot. The raw position-velocity array for this object is shown in Fig. 1, from which the quality of the data can be appreciated. Similarly,

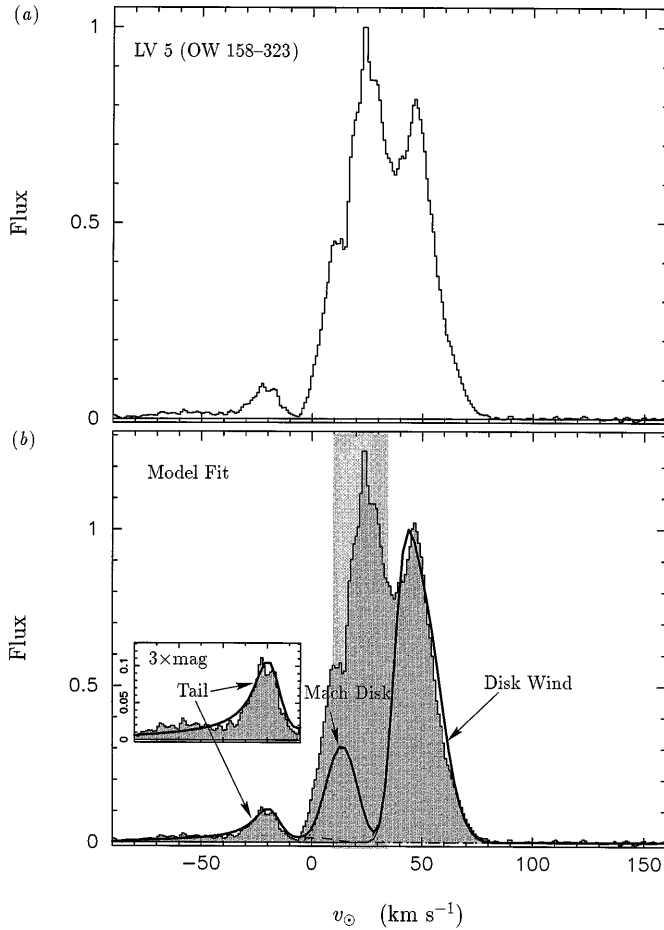


**Fig. 2a and b.** [O III] 5007 Å line profile of LV 5 (OW 158–323). **a** Observed profile. **b** Comparison with model profile (heavy solid line). The different components of the model are indicated by the light solid line (photoevaporated wind), dotted line (Mach disk) and dashed line (swept-back tail). Inset box shows 3×magnification of the blue wing. The region of the spectrum that may be uncertain due to background subtraction is indicated by the light gray rectangle.

for the other objects, portions of the spectra in the heliocentric velocity range  $v_{\odot} = 15\text{--}35 \text{ km s}^{-1}$  are very uncertain.

The background subtraction was carried out as follows. For each emission knot, a spatial segment along the slit  $\Delta x$  was isolated that completely covered the knot emission. This knot segment was divided into 3 sub-segments. Two background segments were then extracted from the spectra to each side of the knot segment and spatially contiguous with it. For each wavelength, the background from these two segments was linearly interpolated across the knot segment and subtracted from each sub-segment separately. The background-subtracted sub-segments were then added together to give the background-subtracted knot spectra shown in Figs. 2 and 3. Although this subtraction technique can be sensitive to non-linearity in the CCD detector, we find that the peak count rate over 4 binned pixels is 28 000 in the bright background profiles near the systemic radial velocity. This is significantly less than the saturation

**Table 1.** Parameters of the longslit spectroscopic observations.

Name <sup>a</sup>	LV#	slit <sup>b</sup>	$\Delta y^c$	$\Delta x^d$	$\Delta v^e$	$\phi^f$
OW 168–326E	1	S1	0.81	2.0	9.0	170
OW 167–317	2	S2	0.81	2.0	9.0	80
OW 163–317	3	10	0.38	2.7	6.0	170
OW 158–323	5	12	0.38	0.9	9.0	4
OW 171–334	–	2	0.38	3.0	6.0	170

<sup>a</sup> Coordinate-based designation (O’Dell & Wen 1994).

<sup>b</sup> Slit label, following Massey & Meaburn (1995)

<sup>c</sup> Width of slit (arcsec).

<sup>d</sup> Length of slit segment used for extracted spectrum (arcsec).

<sup>e</sup> Velocity resolution ( $\text{km s}^{-1}$ ).

<sup>f</sup> Slit position angle (degrees).

**Table 2.** Parameters of model fits to the line profiles.

Name <sup>a</sup>	LV#	$\alpha^b$	$\beta^b$	$\theta_0^b$	$\lambda$	$\delta^c$
OW 168–326E	1	73	-40	23	25	-1.4
OW 167–317	2	74	-23	34	50	0.0
OW 163–317	3	104	29	29	20	-1.2
OW 158–323	5	109	-92	63	170	0.5
OW 171–334	–	104	11	34	150	-0.8

<sup>a</sup> Coordinate-based designation (O’Dell & Wen 1994).

<sup>b</sup> In degrees.

<sup>c</sup> Slit displacement from proplyd center (arcsec).

value of 64 000, so we are confident that the detector response is highly linear.

## 2.2. Model Profiles

Simulated spectra were generated from the proplyd models of Paper I, using the technique outlined in Henney (1996). The models consist of a circumstellar disk around a low mass star, from the illuminated face of which flows a transonic wind due to photoionization by the O7 star  $\theta^1$  Ori C. This disk wind in turn interacts with the stellar wind from  $\theta^1$  Ori C, forming a blunt Mach disk where the ram pressure of the two winds balance, together with a long tail where the disk wind material is swept back by the stronger wind from the O star.

The predicted line profiles are affected by five parameters. Two of these are the parameters that describe the proplyd model:  $\lambda$ , which is the ratio of the momentum flux of newly ionized material entering the base of the disk wind to the momentum flux in the wind of  $\theta^1$  Ori C, and  $\theta_0$ , which is the angle between the disk normal and the direction to  $\theta^1$  Ori C. In addition, there is the orientation of the proplyd with respect to the observer (characterized by an inclination angle  $\alpha$  and an azimuthal angle  $\beta$ ) and the displacement of the slit center from the position of the center of the proplyd.

For each object, the slit parameters from Table 1 are used and the model parameters, orientation and slit position are varied in an attempt to find the best fit to the line profile. A sound speed of  $13 \text{ km s}^{-1}$  is used (appropriate for ionized gas at  $10^4 \text{ K}$ ) and a systemic heliocentric velocity of  $27 \text{ km s}^{-1}$  is assumed for each

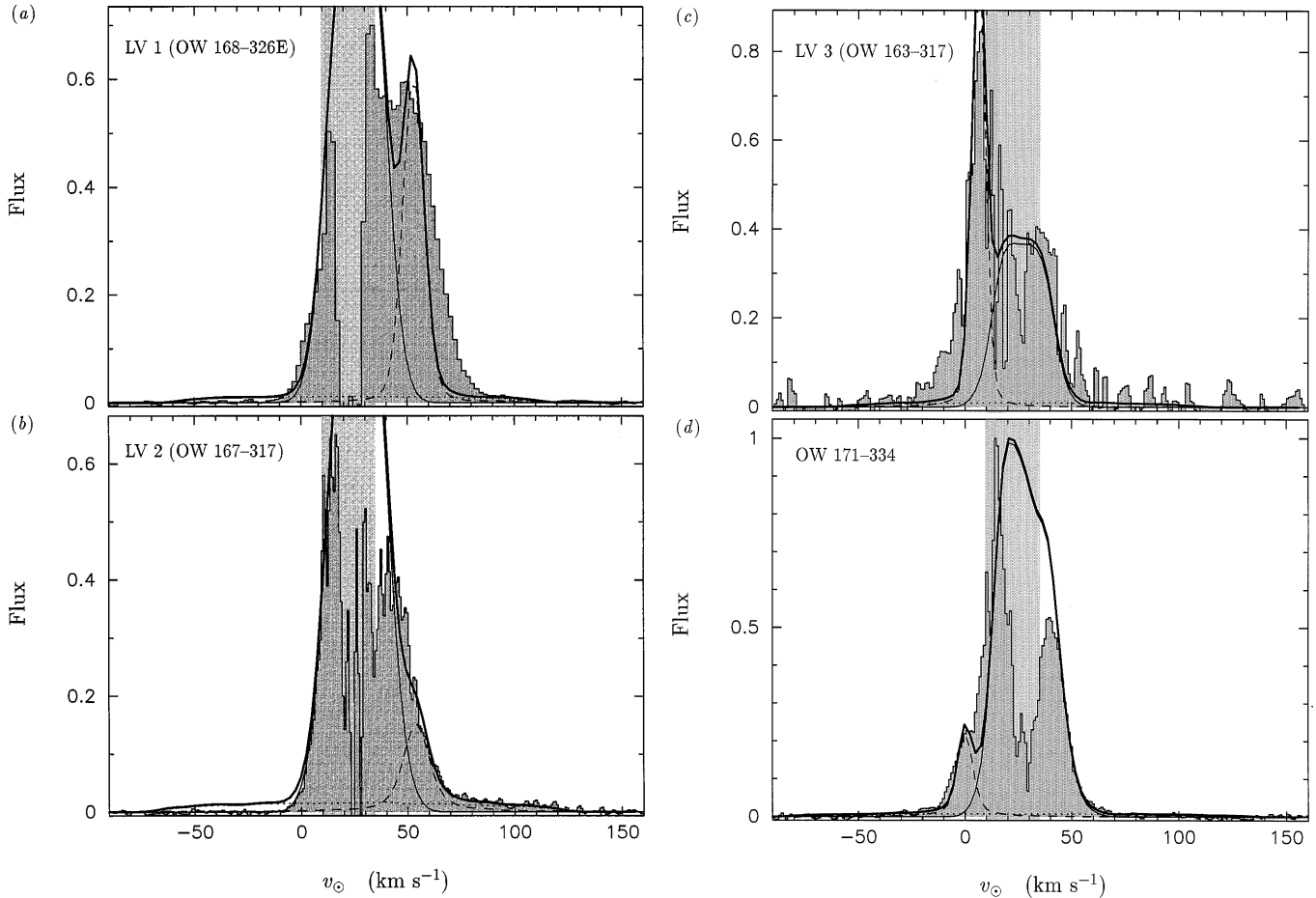


**Fig. 3a–d.** Comparison of observed [O III] 5007Å line profiles of other proplyds (gray histogram) with the models (heavy solid line). Model components as in Fig. 2b. The region of the spectrum that may be uncertain due to background subtraction is indicated by the light gray rectangle. **a** LV 1 (OW 168–326E). **b** LV 2 (OW 167–317). **c** LV 3 (OW 163–317). **d** OW 171–334.

proplyd (corresponding to the velocity of the Orion molecular cloud). The fits would not be substantially improved by allowing peculiar motions of up to  $5 \text{ km s}^{-1}$ . Since the absolute positions on the sky of the spectrograph slits are rather uncertain, we have allowed displacements of the slit by up to one half of the seeing width from the fiducial positions indicated in Fig. 1 of Massey & Meaburn (1995).

The resultant parameters of the best-fit models are shown in Table 2 and the fits themselves are shown superimposed on the observed spectra in Figs. 2 and 3. The model line profiles have three components. The brightest is due to the photoevaporated wind itself and is always close to the systemic velocity. There is also a faint, usually broad, component due to the Mach disk (where the disk wind interacts with  $\theta^1$  Ori C’s wind) and a brighter, more peaked component that is due to the swept-back tail. These three components are shown in the figures by light solid, dotted and dashed lines respectively.

The bulk of the material in the photoevaporated wind moves at only slightly supersonic velocities, so that the Doppler shift of the peak of the wind emission depends only on the angle

between the normal to the disk and the line of sight and is very approximately given by  $c_0(\cos \alpha + \sin \theta_0 \sin \beta \sin \alpha)$ . Note that, since this depends on all three of the angular parameters, it would be impossible to find a unique fit to the wind component of the line profile alone, even in the absence of background subtraction problems near the systemic velocity. The width and shape of the wind component also depend on the angular parameters but in a rather complicated way, especially for instances where the base of the wind is partially occulted by the opaque circumstellar disk.

However, if the tail component of the line profile can also be identified, then a reasonably unique fit can be determined. This is because the ratio of the intensities of the wind component to the tail component depends almost exclusively on the parameter  $\lambda$ , whereas the Doppler shift of the peak in the tail component depends mainly on  $\alpha$ , but only very weakly on  $\lambda$  and not at all on the other angular parameters. The relative intensity of the Mach disk component is rather insensitive to all the model parameters except that, for slits that are more or less perpendicular to the

proplyd axis, it does depend on the position of the slit. Hence, we can fit the models to the observations in a systematic way.

### 3. Discussion

We first focus attention on LV 5 (OW 158–323) since the observed spectrum of this object is of much higher quality than the others. The line profile, illustrated in Fig. 2a, shows three strong components close to the systemic velocity, at  $v_{\odot} = 10, 22$  and  $35 \text{ km s}^{-1}$ , together with a weaker blue-shifted component at  $v_{\odot} = -20 \text{ km s}^{-1}$ , which possesses a wing extending out to  $v_{\odot} = -70 \text{ km s}^{-1}$ . Because of uncertainties in subtraction of the strong and highly variable background (see Fig. 1), it is possible that the  $22 \text{ km s}^{-1}$  peak is spurious and hence we ignore it in our model fits. It is obviously not entirely satisfactory to exclude the  $10$  to  $35 \text{ km s}^{-1}$  region from our fit, but in order to reliably isolate this portion of the proplyd spectrum from the background nebular emission, much higher spatial resolution is necessary than is available from ground-based observations.

Our model reproduces well the redmost peak, together with the blue peak and wing. However, the  $10 \text{ km s}^{-1}$  peak, although present in our model (due to the Mach disk) is not strong enough. We note that in order to obtain a peaked rather than broad Mach disk component, a rather special combination of parameters is required. In particular, it is necessary that  $\alpha + \theta_0 \simeq 180^\circ$  and that  $\beta \simeq -90^\circ$ . This leads to a value for the inclination of the disk normal with respect to the direction of  $\theta^1$  Ori C of  $\theta_0 = 63^\circ$  for LV 5, which is at the upper limit of that allowed by our simple dynamical model of the proplyds (see Paper I).

Apart from shortcomings in our dynamical model, one factor that could effect the proplyd line profiles and which is not considered in this paper is dust scattering in the photoevaporated wind. The dust optical depth to the base of the wind in our models is of order  $0.2$ – $1.0$  at the wavelength of the  $[\text{O III}]$   $5007\text{\AA}$  line and this could have a substantial effect on the wind component of our model profile (c.f. Henney 1994; Henney & Axon 1995). Since the wind is both divergent and accelerating, any scattered component will be red-shifted with respect to the direct emission from the wind. Preliminary results of detailed modelling of this process (to be presented in a subsequent paper) show that the principal effect on the line profiles is to broaden the component due to the photoevaporated wind by  $10$ – $20 \text{ km s}^{-1}$ .

From the position-velocity array of LV 5 (Fig. 1) it is apparent that the blue-shifted emission peak is more extended spatially than either the far blue wing or the red-shifted peak. We find that our model spectrum also shows this feature, which arises because the blue peak is due to the swept-back tail of the proplyd, which is its most spatially extended part.

Turning now to the other proplyds, illustrated in Figs. 3a–d, the observations are somewhat poorer (mainly because of problems with background subtraction) and all have unreliable portions somewhere in the range  $v_{\odot} = 15$ – $35 \text{ km s}^{-1}$  (indicated by light gray shading on the figures). The quality of the model fits is variable, ranging from very good in the case of OW 163–317 to very poor in the case of LV 1 (OW 168–326E). In other cases, such as LV 2 (OW 167–317), the fit to the red portion of the

spectrum is good but the model predicts an extended blue wing, which is not observed.

The deduced values of the parameter  $\lambda$  for our fitted models (Table 2) are all reasonable, lying in the range expected for proplyds at a distance from  $\theta^1$  Ori C of  $0.01$ – $0.05$  parsecs. They are, however, a little higher than the values ( $10$ – $30$ ) found by fitting the morphology of the proplyds in Paper I. In addition, the angles  $\alpha$ ,  $\beta$  and  $\theta_0$  of the fits listed in Table 2 are, in general, different from the fits to the same objects found in Paper I. However, we feel that the line profiles are a much more effective discriminant of the model parameters than the morphologies, and indeed the fits found here still show reasonable agreement with the observed morphologies.

In summary, our proplyd model is successful in accounting for most of the features in the  $[\text{O III}]$   $5007\text{\AA}$  line profiles of the five emission line knots presented here. It is hoped that the remaining discrepancies between theory and observation will be removed by improvements in the model (for instance, a fuller treatment of the effects of gravity on the disk wind and a more detailed calculation of the flow in the tail) and by a more realistic treatment of the radiative transfer, including dust absorption and scattering.

*Acknowledgements.* It is a pleasure to thank Dave Berry for help during the extraction of the line profiles. WJH and ACR acknowledge financial support from DGAPA project IN105295.

### References

- Churchwell, E. B., Felli, M., Wood, D. O. S. & Massi, M. 1987, *ApJ*, 321, 516  
 Felli, M., Taylor, G. B., Catarzi, M., Churchwell, E. & Kurtz, S. 1993, *A&AS*, 101, 127  
 Garay, G., Moran, J. M. & Reed, M. J. 1987, *ApJ*, 314, 535  
 Henney, W. J. 1994, *ApJ*, 427, 288  
 Henney, W. J. & Axon, D. J. 1995, *ApJ*, 454, 233  
 Henney, W. J. 1996, *RevMexAA*, 32, 3  
 Henney, W. J., Raga, A. C., Lizano, S. & Curiel, S. 1996, *ApJ*, in press (Paper I)  
 Laques, P. & Vidal, J. L. 1979, *A&A*, 73, 97  
 Massey, R. M. & Meaburn, J. 1993, *MNRAS*, 262, L48  
 Massey, R. M. & Meaburn, J. 1995, *MNRAS*, 273, 615  
 Meaburn, J. 1988, *MNRAS*, 233, 791  
 Meaburn, J., Massey, R. M., Raga, A. C. & Clayton, C.A. 1993, *MNRAS*, 260, 625  
 McCaughrean, M. J. 1988, PhD thesis, University of Edinburgh  
 McCaughrean, M. J. & Stauffer, J. R. 1994, *AJ*, 108, 1382  
 McCullough, P. R., Fugate, R. Q., Christou, J. C., Ellerbroek, B. L., Higgins, C. H., Spinhirne, R. A., Cleis, R. A., & Moroney, J. F. 1995, *ApJ*, 438, 394  
 O’Dell, C. R., Wen, Z., & Hu, X. 1993, *ApJ*, 410, 696  
 O’Dell, C. R. & Wen, Z. 1994, *ApJ*, 436, 194